Nonlinear ultrasonic analysis inspired by phase-based motion magnification

Peipei Liu, Zhanxiong Ma, Jinho Jang, Hoon Sohn

Peipei Liu, Zhanxiong Ma, Jinho Jang, Hoon Sohn, "Nonlinear ultrasonic analysis inspired by phase-based motion magnification," Proc. SPIE 12488, Health Monitoring of Structural and Biological Systems XVII, 124880L (25 April 2023); doi: 10.1117/12.2657061

SPIE.

Event: SPIE Smart Structures + Nondestructive Evaluation, 2023, Long Beach, California, United States

Nonlinear ultrasonic analysis inspired by phase-based motion magnification

Peipei Liu[a,b], Zhanxiong Ma[a], Jinho Jang[a], Hoon Sohn[*a,b]
[a] Department of Civil and Environmental Engineering, Korea Advanced Institute of Science and Technology, Daejeon, 34141, Republic of Korea; [b] Center for 3D Printing Nondestructive Testing, Korea Advanced Institute of Science and Technology, Daejeon, 34141, Republic of Korea

ABSTRACT

Nonlinear ultrasonic modulation is favored for early-stage fatigue crack detection by inspecting the modulation components at the sum and difference of two distinct input frequencies. However, it is difficult to extract the modulation components using a conventional spectral density function considering the modulation components can be easily buried under noisy environments. In this study, we proposed a new nonlinear ultrasonic analysis method inspired by phase-based motion magnification. First, a one-dimensional time-domain ultrasonic signal is filtered to remove the large motions of the primary linear response components. Then, the filtered signal is used to construct a two-dimensional video and the phase-based motion magnification algorithm is applied to enhance the movements at the predetermined modulation frequencies inside the video. This step is achieved by phase denoising and phase magnification, which supports large magnification factors and is significantly insensitive to noise. Finally, an amplified one-dimensional signal is extracted from the two-dimensional video and can be used for further nonlinear ultrasonic analysis. The proposed method was successfully validated with a group of synthetic data at different noise levels. Additionally, we have also successfully applied the proposed method for fatigue crack detection in a steel padeye.

Keywords: nonlinear ultrasonic modulation, phase-based motion magnification, fatigue crack, padeye

1. INTRODUCTION

Nonlinear ultrasonic modulation indicates ultrasonic components whose frequencies appear at sum and difference of the input frequencies, and it can provide a much-improved sensitivity in micro defect detection compared to classical linear ultrasonic techniques [1]. Nonlinear ultrasonic modulation has been widely studied for fatigue crack inspection in metal and concrete [2, 3], delamination detection in composites [4], and recently for porosity evaluation and microstructure characterization in additively manufactured objects [5, 6].

A technical hurdle for nonlinear ultrasonic modulation is that it is difficult to identify subtle modulation components from ultrasonic responses measured in noisy environments. Attempts have been made to enhance the defect detection reliability with nonlinear ultrasonic modulation, including (1) input frequency sweeping to find an optimal frequency combination that can intensify the defect-induced modulation [7]; (2) signal denoising by filtering a spatial signal network (e.g., acquisition by laser scanning) [8, 9]; (3) noise suppression by bispectrum or spectral correction analysis [10, 11]; and (4) sequential pattern learning via artificial neural networks (e.g., long short-term memory) [12, 13]. The efficacy to capture the nonlinear modulation responses, however, are limited because these methods focus solely on noise suppression, not to mention that some methods demand a high time cost for signal acquisition.

This study proposes a new nonlinear ultrasonic analysis method inspired by phase-based motion magnification, which actively enhances the nonlinear modulations and suppresses noise. The proposed method offers the following advantages: (1) A one-dimensional (1D) time-domain ultrasonic signal is converted to a two-dimensional (2D) video with automated parameter selection. (2) Subtle nonlinear modulation responses are amplified by phase manipulation and magnification of the converted 2D video. (3) Time-domain noise can also be effectively suppressed by spatial phase denoising of the converted video. The validation of the proposed method was performed with synthetic ultrasonic signals and the experiment data obtained from a steel padeye sample under cyclic loading test.

[*] hoonsohn@kaist.ac.kr; phone (+82) 42-350-3625; fax (+82) 42-350-8480; ssslab.kaist.ac.kr

Health Monitoring of Structural and Biological Systems XVII, edited by Paul Fromme, Zhongqing Su, Proc. of SPIE Vol. 12488, 124880L
 · 0277-786X · doi: 10.1117/12.2657061

2. METHODOLOGY

For a structure excited at two distinct frequencies (f_a and f_b), its 1D time-domain response s is composed of the linear response s_l (f_a, f_b), nonlinear response s_m ($f_b \pm f_a$, if the structure behaves nonlinearly), and noise s_n. The large motions of the primary linear response s_l can be easily separated by bandpass filtering of s, and we obtain a small-motion signal s_s ($s_s = s_m + s_n$).

The small-motion signal s_s is then used to construct a 2D video and phase-based motion magnification algorithm is applied to enhance the movements at the predetermined modulation frequencies inside the video. This procedure consists of the following steps (Figure 1(a)):

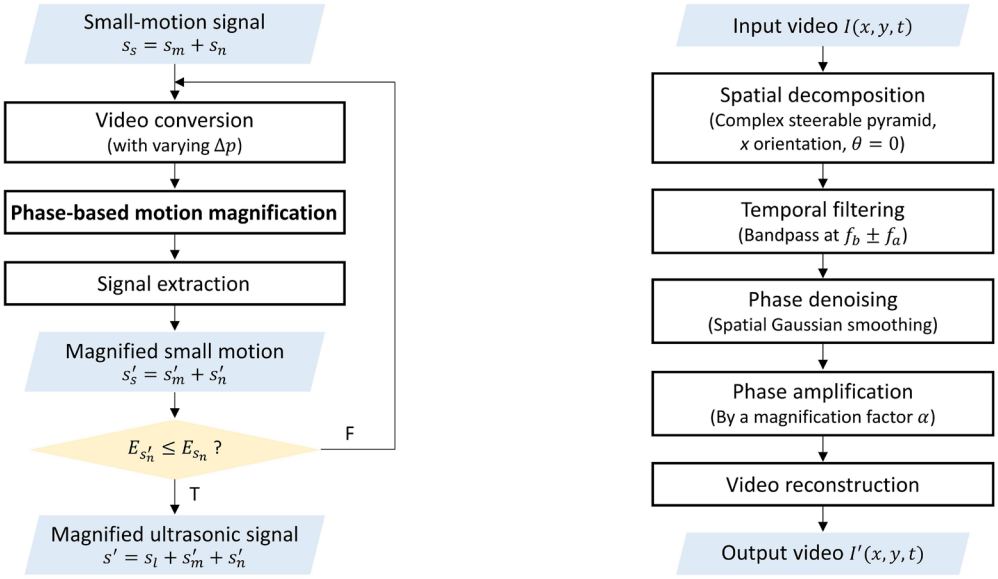

Figure 1. (a) Overview of nonlinear ultrasonic enhancement of the separated small-motion signal s_s, and (b) Process of phase-based motion magnification.

(1) To convert s_s into a 2D video $I(x, y, t)$, s_s is divided into N segments. Each segment contains M data points and is used to individually establish the pixel movement in the video along a designated x orientation and at a fixed y position.

$$I\left(\frac{s_s\big((j-1)M+i\big)}{max|s_s|}\cdot\Delta p, j+1, i\Delta t\right)=1 \qquad 0<i\leq M, 0<j\leq N \tag{1}$$

where the pixel scale Δp indicates the largest pixel movement in the constructed video, and Δp is to be automatically determined by considering the noise level for each measurement. Note that M is selected to include the integer periods of $f_b \pm f_a$. $I(x, y, t) = 0$ is assigned for other pixels, and the size of $I(x, y, t)$ is set to $(N + 2, N + 2, M)$ in this study.

(2) Phase-based motion magnification is adopted to $I(x, y, t)$ [14]. As shown in Figure 1(b), complex steerable pyramids are used to decompose $I(x, y, t)$ into multiple spatial sub-bands $S_{\omega,\theta}(x, y, t)$.

$$\tilde{S}_{\omega,\theta}(k_x, k_y, t) = \tilde{I}(k_x, k_y, t)\Psi_{\omega,\theta}(k_x, k_y) \tag{2}$$

where $\tilde{S}_{\omega,\theta}(k_x, k_y, t)$ is the spatial discrete Fourier transform (DFT) of the decomposed sub-band $S_{\omega,\theta}(x, y, t)$, and $\tilde{I}(k_x, k_y, t)$ is the spatial DFT of each frame in video $I(x, y, t)$. $\Psi_{\omega,\theta}(k_x, k_y)$ is the frequency domain transfer function of the complex steerable pyramid at spatial scale ω and orientation θ. Here, only $S_{\omega,0}(x, y, t)$ ($\theta = 0$) are to be further processed because s_s is converted to the pixel movement along the x orientation.

$S_{\omega,0}(x, y, t)$ allows access to local amplitude and phase in video frames, and the nonlinear response induced subtle motions can be amplified by filtering and modifying of the phase variation. For clear explanation, we first simplify $S_{\omega,0}(x, y, t)$ to a 1D profile $S_{\omega,0}(x, t)$ under global translation $\delta(t)$ ($S_{\omega,0}(x, t) = S_{\omega,0}(x + \delta(t))$). By Fourier series decomposition, $S_{\omega,0}(x, t)$ can be written as

$$S_{\omega,0}(x,t) = \sum_{f=-\infty}^{+\infty} S_f(x,t) = \sum_{f=-\infty}^{+\infty} A_f e^{i2\pi f(x+\delta(t))} \tag{3}$$

where $S_f(x,t)$ corresponds to the component at temporal frequency f with an amplitude of A_f. Here, since $S_f(x,t)$ is a complex sinusoid, its phase $2\pi f(x+\delta(t))$ contains motion information $\delta(t)$. Temporal filtering is applied to $2\pi f(x+\delta(t))$ to isolate the phase $B_f(x,t)$ at $f_b \pm f_a$.

$$B_f(x,t) = 2\pi(f_b \pm f_a)\delta(t) \tag{4}$$

Because noise s_n can alter $\delta(t)$ and cause $B_f(x,t)$ to be noisy, phase denoising is applied to each video frame by low-passing $B_f(x,t)$ with amplitude-weighted spatial Gaussian smoothing.

$$B_f^s(x,t) = \frac{(B_f(x,t)A_f) * \mathrm{K}_\rho(x)}{A_f * \mathrm{K}_\rho(x)} = 2\pi(f_b \pm f_a)\delta^s(t) \tag{5}$$

where $\mathrm{K}_\rho(x)$ is a Gaussian kernel given by e^{-x^2/ρ^2}, ρ is chosen to be equal to the spatial domain filter width ($\rho = N+2$), and $\delta^s(t)$ is the denoised translation. Indeed, since each segment of s_s includes integer periods of $f_b \pm f_a$, the spatial phase variations among the pixels are caused only by noise s_n.

The spatially-filtered phase $B_f^s(x,t)$ is then multiplied by a magnification factor α, and added to the phase of $S_f(x,t)$ to obtain motion magnified $S'_f(x,t)$.

$$S'_f(x,t) = S_f(x,t)e^{i\alpha B_f^s(x,t)} = A_f e^{i2\pi f(x+\delta(t)+\alpha\delta^s(t))} \qquad (f = f_b \pm f_a) \tag{6}$$

where $S'_f(x,t)$ at $f_b \pm f_a$ becomes $S_f(x+(1+\alpha)\delta(t))$ without noise s_n. In this case, the motion at $f_b \pm f_a$ is magnified $1+\alpha$ times. The amplified sub-band $S'_{\omega,0}(x,t)$ can be achieved by a sum of $S'_f(x,t)$.

The above process can be easily generalized to a 2D sub-band $S_{\omega,0}(x,y,t)$ with local motions $\delta(x,y,t)$ to obtain the amplified sub-band $S'_{\omega,0}(x,y,t)$. The $S'_{\omega,0}(x,y,t)$ are then collapsed over all the spatial scales.

$$\tilde{I}'(k_x,k_y,t) = \sum \tilde{S}'_{\omega,0}(k_x,k_y,t)\Psi_{\omega,0}(k_x,k_y) \tag{7}$$

where $\tilde{S}'_{\omega,\theta}(k_x,k_y,t)$ is the spatial DFT of $S'_{\omega,\theta}(x,y,t)$. The motion magnified video $I'(x,y,t)$ can be obtained by inverse spatial DFT of $\tilde{I}'(k_x,k_y,t)$.

(3) A magnified signal s_s' ($s_s' = s_m' + s_n'$) can be extracted from $I'(x,y,t)$ by reversing the process of Equation (1). The steps in Figure 1(a) are repeated with varying pixel scale Δp until the following condition is satisfied.

$$E_{s_n'} \le E_{s_n} \tag{8}$$

where $E_{s_n'}$ and E_{s_n} are the energies of s_n' and s_n, i.e., the energies of s_s' and s_s minus $f_b \pm f_a$ components, respectively. The final magnified ultrasonic signal is acquired as $s' = s_l + s_s'$ with enhanced nonlinear modulation responses.

3. VALIDATION WITH SYTHETIC DATA

3.1 Description of synthetic ultrasonic signals

To generate synthetic ultrasonic signals, the linear components s_l were unit amplitude sinusoidal signals, $s_l = \sin(2\pi f_a t) + \sin(2\pi f_b t)$ ($f_a = 45$ kHz and $f_b = 206$ kHz), and the corresponding nonlinear modulation components were set as $s_m = 0.01 \times \sin(2\pi(f_b \pm f_a)t)$. Gaussian white noise s_n was created with respect to s_m with a signal-to-noise ratio (SNR) defined as

$$\mathrm{SNR} = 10\log\frac{E_{s_m}}{E_{s_n}}\ (\mathrm{dB}) \tag{9}$$

where E_{s_m} and E_{s_n} are the energies of s_m and s_n, respectively. Here, $\mathrm{SNR} = -47$ was chosen because s_m can by drowned by s_n in the frequency domain. Correspondingly, synthetic intact and damage ultrasonic signals were generated as

$$\begin{aligned} s_i &= s_l + s_n \\ s_d &= s_l + s_m + s_n \end{aligned} \tag{10}$$

where both s_i and s_d were discretely sampled at 1 MHz for 100 ms.

3.2 Test results with synthetic ultrasonic signals

For motion magnification, the synthetic signals were divided into 100 segments ($M = 1000$, $N = 100$), and the magnification factor was set to $\alpha = 2$. The automatically selected pixel scale Δp was 5 for both s_i and s_d. Figure 2 shows the spectral plots of s_i and s_d before and after motion magnification. It can be seen in that $E_{s_n'}$ and E_{s_n} (Equation (8)) remained at a similar level, and the modulation components s_m were hardly observable in s_d (Figure 2(b)). After motion magnification of s_d, s_m was amplified and clearly seen in the spectral plot of the magnified s_d' (Figure 2(b)). s_m' in s_d' was magnified approximately $3(= 1 + \alpha)$ times (9 times in the spectral plot). On the other hand, since there was no s_m in s_i, the spectral values at $f_b \pm f_a$ did not alter much after motion magnification (Figure 2(a)).

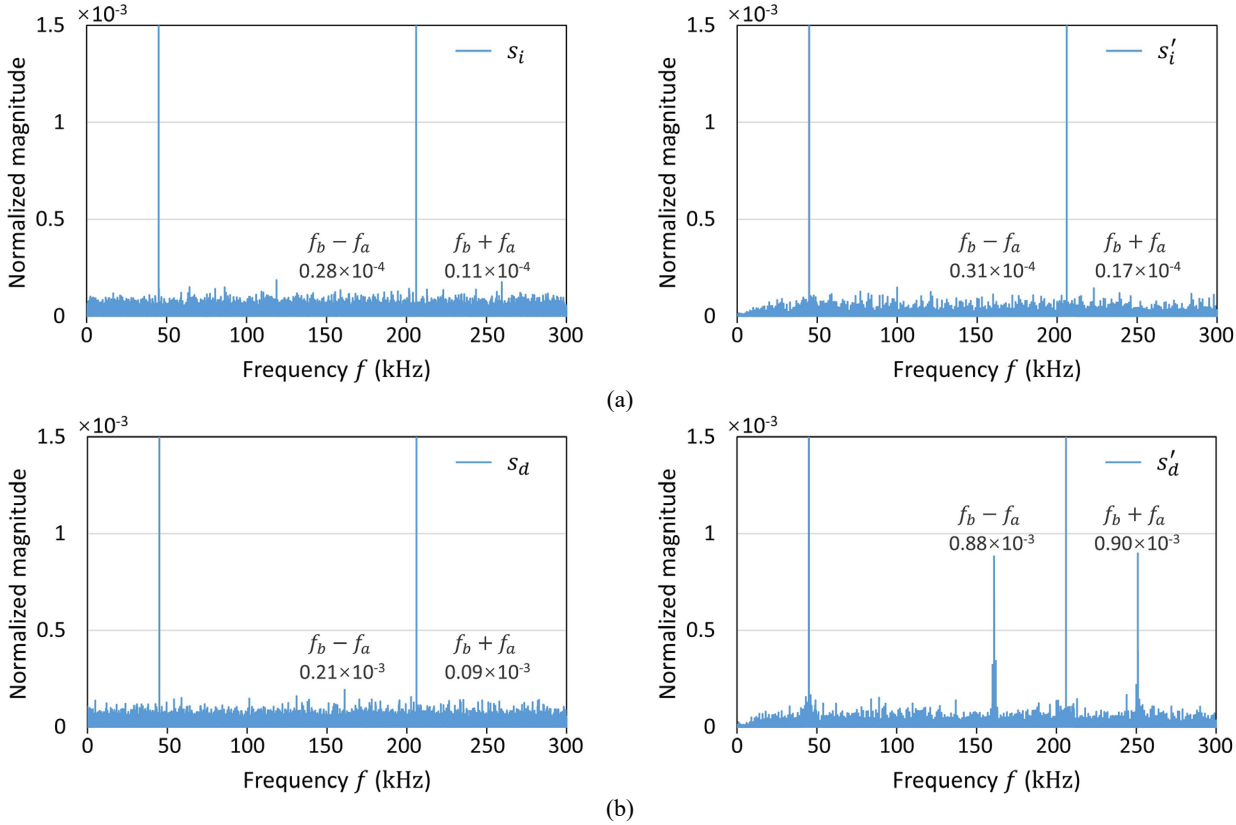

Figure 2. Spectral plots of synthetic signals before and after motion magnification. (a) s_i and magnified s_i', and (b) s_d and magnified s_d'.

A nonlinear modulation parameter β was calculated to quantitatively evaluate the performance of the proposed motion magnification-based method, and β is defined as [15]

$$\beta \approx \frac{A_{f_b - f_a} + A_{f_b + f_a}}{A_{f_a} A_{f_b}} \tag{11}$$

where A_{f_a}, A_{f_b}, $A_{f_b - f_a}$, and $A_{f_b + f_a}$ are the spectral values at the input and modulation frequencies, respectively. The β value calculated from s_d' ($\beta = 1.78 \times 10^{-3}$) increased approximately 6 times compared to the β value of s_d ($\beta = 0.30 \times 10^{-3}$), while the β values remained barely changed for the synthetic intact signal ($\beta = 0.39 \times 10^{-3}$ for s_i, and $\beta = 0.48 \times 10^{-3}$ for s_i').

Figure 3(a) shows the spectral plot of s_i magnified without the phase denoising process in motion magnification (Figure 1(b)). By comparing between Figure 2(a) and Figure 3(a), it clearly demonstrates that the incorrect motions of noise s_n at $f_b \pm f_a$ were amplified once phase denoising process was omitted, and the deviation of the β value between s_i and s_i' increased ($\beta = 0.81 \times 10^{-3}$ for s_i' without phase denoising).

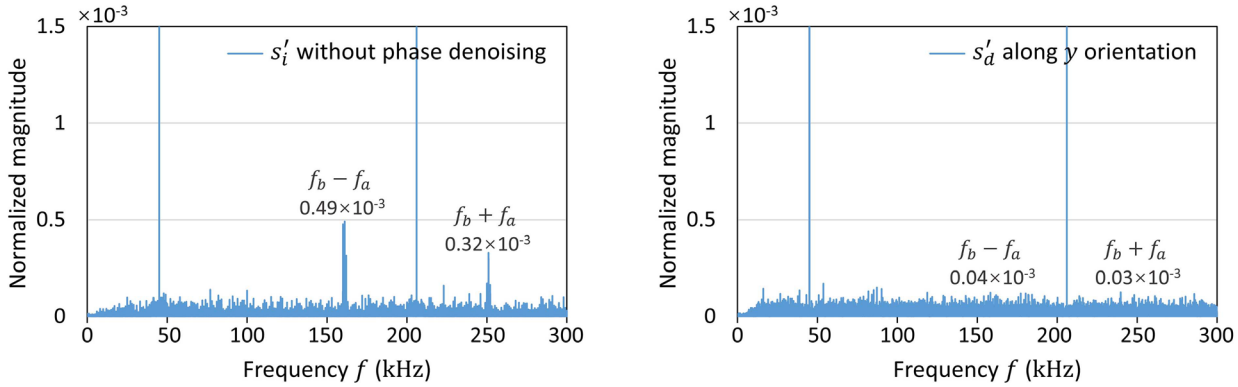

Figure 3. (a) Spectral plot of s_i magnified without phase denoising, and (b) Spectral plot of s_d magnified along the y orientation.

Additionally, Figure 3(b) shows the spectral plot of s_d magnified with the sub-bands along the y orientation ($\theta = \pi/2$). It verifies that the nonlinear components s_m only existed in the sub-bands $S_{\omega,0}(x, y, t)$ along the x orientation (Figure 2(b)). This is because when the time-domain signal is converted to a video in the proposed method, the pixel movement is designated only along the x orientation (Equation (1)). Therefore, only $S_{\omega,0}(x, y, t)$ decomposed along the x orientation are magnified for nonlinear signal enhancement.

4. FATIGUE CRACK DETECTION IN A PADEYE

4.1 Experimental setup

The proposed method was further validated with the experimental data acquired from a SM490 steel padeye sample under a cyclic loading test. The geometrical information of the padeye sample is shown in Figure 4(a). The cyclic loading test was carried out using a universal testing machine (UTM, Instron 8801) with a cycle rate of 10 Hz, a maximum load of 50 kN, and a stress ratio of 0.1. Fatigue cracks initiated from the edge of the pin hole after 120 k fatigue cycles and the padeye sample failed at 230 k fatigue cycles (Figure 4(b)).

Three piezoceramic transducers (APC International, APC850) were attached on the cheek plate of the padeye sample (Figure 4(a)), and ultrasonic signals were measured periodically during the cyclic loading test with a National Instruments system [11]. Ultrasonic waves were generated via PZT A and PZT B at $f_a = 50$ kHz and $f_b = 193$ kHz, and the corresponding ultrasonic responses s were measured with PZT C with a 1 MHz sampling rate for 100 ms at different fatigue cycles.

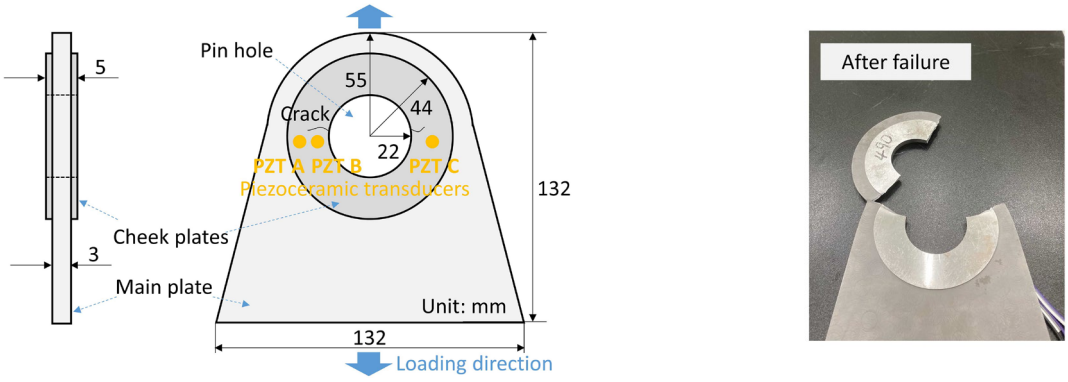

Figure 4. (a) Geometrical dimensions of the padeye, and (b) Padeye failure at 230 k fatigue cycles.

4.2 Experimental results

For motion magnification, each measured signal s was divided into 100 segments ($M = 1000, N = 100$), and the magnification factor was set to $\alpha = 2$. Figures 5(a) and 5(b) show the spectral plots of s and the magnified s' at 30 k and 150 k fatigue cycles, respectively. The pixel scale Δp was selected as 5 and 6 for signals s measured at 30 k and 150 k fatigue cycles, respectively. Here, the pixel scale Δp varied because the signal composition (i.e., nonlinear responses and noise) altered in measurements at different fatigue cycles. It is clearly demonstrated in Figure 5(a) that nonlinear modulations at $f_b \pm f_a$ became observable in s' after motion magnification. It was inferred that the nonlinear responses at 30 k fatigue cycles were caused by the inherent material nonlinearity of the padeye sample. At 150 k fatigue cycles, fatigue cracks initiated and were growing from the pin hole edge of the sample. Correspondingly, the nonlinear modulation components increased owing to the intensification of crack opening and closing, as shown in Figure 5(b).

The β values calculated from s were 0.55×10^{-4} and 0.80×10^{-4} at 30 k and 150 k fatigue cycles; and the β values from s' were 0.17×10^{-3} and 1.01×10^{-3} at 30 k and 150 k fatigue cycles, respectively. The increase of β before and after crack initiation was approximately 1.45 times in s but 5.94 times in the magnified s'.

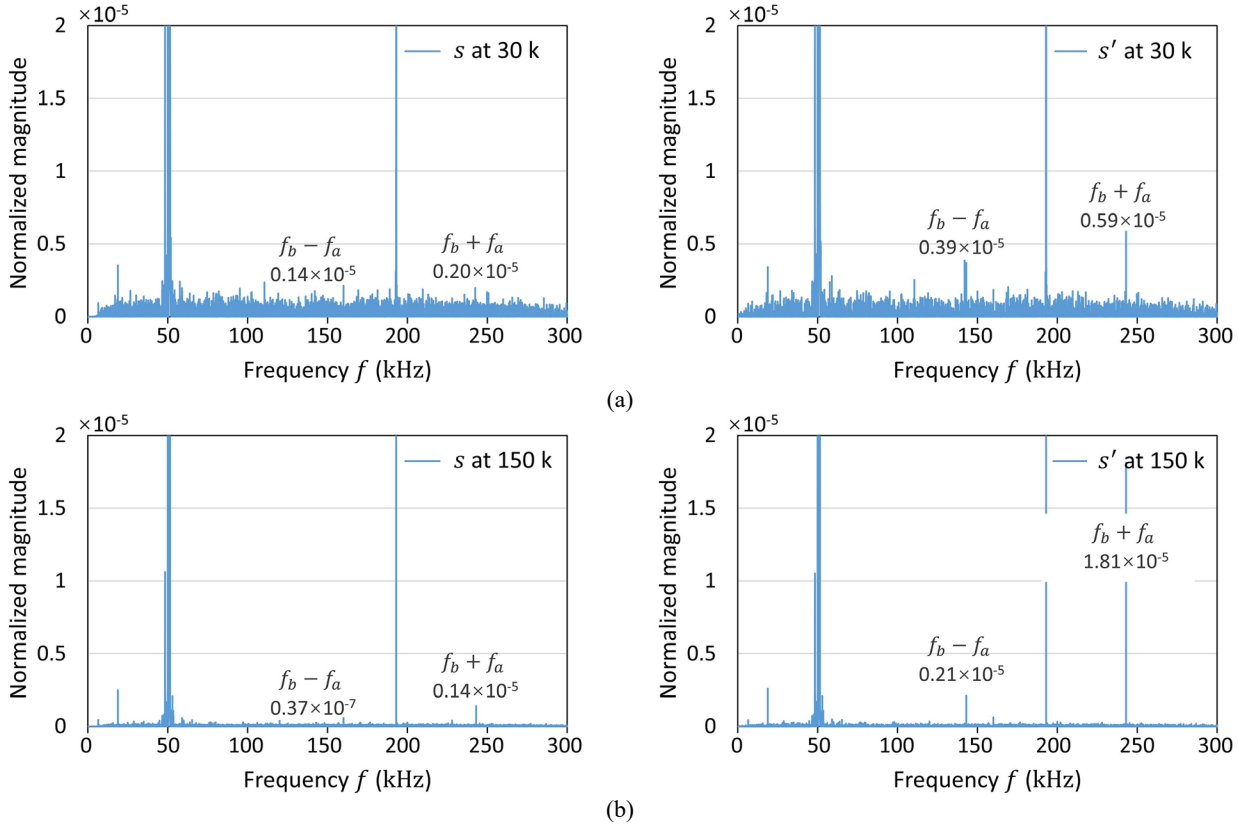

Figure 5. Spectral plots of experimental signals before and after motion magnification measured at different fatigue cycles. (a) 30 k, and (b) 150 k.

5. CONCLUSIONS

In this study, a new nonlinear ultrasonic analysis method was proposed based on phase-based motion magnification. A 2D video was constructed from a 1D time-domain ultrasonic measurement. Subtle motions of the nonlinear responses were amplified by filtering and modifying the temporal- and spatial-phase variations of the constructed 2D video. The magnified ultrasonic signal was then extracted from the magnified 2D video for further nonlinear ultrasonic analysis. A future study is warranted to explore different strategies for time-domain signal conversion into 2D videos, and field applications in noisy environments.

ACKNOWLEDGEMENT

This work was supported by a National Research Foundation of Korea (NRF) grant funded by the Korean government (MSIT) [Grant number 2019R1A3B3067987].

REFERENCES

[1] K.-Y. Jhang, "Nonlinear ultrasonic techniques for nondestructive assessment of micro damage in material: a review," International journal of precision engineering and manufacturing, 10(1), 123-135 (2009).

[2] X. Chen, J.-Y. Kim, K. Kurtis et al., "Characterization of progressive microcracking in Portland cement mortar using nonlinear ultrasonics," NDT & E International, 41(2), 112-118 (2008).

[3] P. Liu, J. Jang, and H. Sohn, "Crack localization by laser-induced narrowband ultrasound and nonlinear ultrasonic modulation," Smart Structures and Systems, An International Journal, 25(3), 301-310 (2020).

[4] B. Boll, E. Willmann, B. Fiedler et al., "Weak adhesion detection–Enhancing the analysis of vibroacoustic modulation by machine learning," Composite Structures, 273, 114233 (2021).

[5] P. Liu, L. Yang, K. Yi et al., "Application of nonlinear ultrasonic analysis for in situ monitoring of metal additive manufacturing," Structural Health Monitoring, 14759217221113447 (2022).

[6] P. Liu, K. Yi, Y. Park et al., "Ultrafast nonlinear ultrasonic measurement using femtosecond laser and modified lock-in detection," Optics and Lasers in Engineering, 150, 106844 (2022).

[7] K. Dziedziech, L. Pieczonka, M. Adamczyk et al., "Efficient swept sine chirp excitation in the non-linear vibro-acoustic wave modulation technique used for damage detection," Structural Health Monitoring, 17(3), 565-576 (2018).

[8] Y. He, K. Wang, L. Xu et al., "Laser ultrasonic imaging of submillimeter defect in a thick waveguide using entropy-polarized bilateral filtering and minimum variance beamforming," Mechanical Systems and Signal Processing, 186, 109863 (2023).

[9] P. Liu, H. Sohn, S. Yang et al., "Fatigue crack localization using noncontact laser ultrasonics and state space attractors," The Journal of the Acoustical Society of America, 138(2), 890-898 (2015).

[10] N. Li, J. Sun, J. Jiao et al., "Quantitative evaluation of micro-cracks using nonlinear ultrasonic modulation method," Ndt & E International, 79, 63-72 (2016).

[11] P. Liu, and H. Sohn, "Development of nonlinear spectral correlation between ultrasonic modulation components," NDT & E International, 91, 120-128 (2017).

[12] J. Jang, H. Sohn, and H. J. Lim, "Spectral noise and data reduction using a long short-term memory network for nonlinear ultrasonic modulation-based fatigue crack detection," Ultrasonics, 129, 106909 (2023).

[13] W. Xu, X. Li, J. Zhang et al., "Ultrasonic signal enhancement for coarse grain materials by machine learning analysis," Ultrasonics, 117, 106550 (2021).

[14] N. Wadhwa, M. Rubinstein, F. Durand et al., "Phase-based video motion processing," ACM Transactions on Graphics (TOG), 32(4), 1-10 (2013).

[15] T. Kundu, J. N. Eiras, W. Li et al., [Fundamentals of nonlinear acoustical techniques and sideband peak count] Springer, (2019).